

POLY(ESTER AMIDE) NANOCOMPOSITES BY IN SITU POLYMERIZATION: KINETIC STUDIES ON POLYCONDENSATION AND CRYSTALLIZATION

L. Morales-Gómez,^{1,2} I. Jones,¹ L. Franco,^{1,2} J. Puiggali^{1,2}

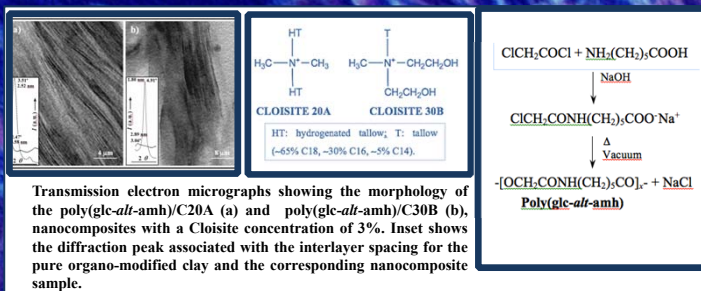
http://psep.upc.edu e-mail: laura.teresa.morales@upc.edu

¹Universitat Politècnica de Catalunya, Departament d'Enginyeria Química, Diagonal 647, 08028-Barcelona
²Centre de Recerca de NanoEnginyeria (CRNE).

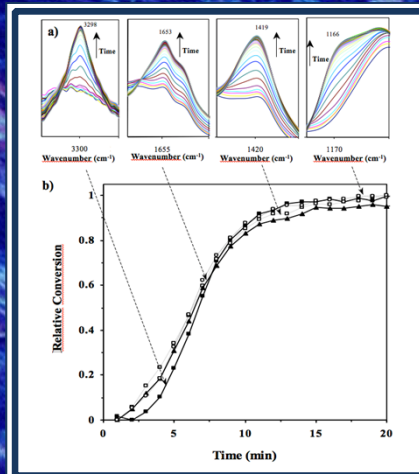


Preparation of nanocomposites by in situ polymerization of sodium chloroacetylaminohexanoate in the presence of cloisite 20A (C20A) or cloisite 30B (C30B) organo-modified montmorillonites was studied. Both clays rendered an intercalated structure that contrasts with the exfoliated structure previously found with the use of the C25A montmorillonite. Polymerization under non-isothermal and isothermal conditions was evaluated by Wide Angle X-ray Diffraction (WAXD) synchrotron radiation and Fourier Transform Infrared Spectroscopy (FTIR) experiments.

The crystallization kinetics of the intercalated C20A and C30B nanocomposites was studied by FTIR and optical microscopy. Layered silicate particles are especially interesting for nanocomposite preparation as they may be dispersed into individual layers with a thickness close to 1 nm to tune surface interactions with the polymer/monomer through exchange reactions with organic and inorganic cations. The final structure of the composite depends on the extent to which the organic matrix and inorganic clay components are made compatible, and varies from an intercalated to a fully exfoliated nanostructure, which has an obvious impact on the final properties. Despite extensive research, the influence of nanocomposite structure on nucleation and crystal growth rate is not entirely clear in view of the conflicting results reported in some cases.

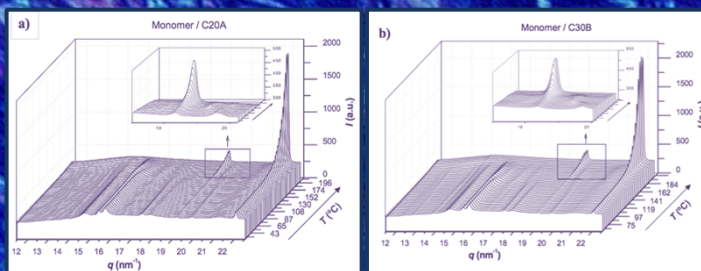


Transmission electron micrographs showing the morphology of the poly(glc-alt-amh)/C20A (a) and poly(glc-alt-amh)/C30B (b), nanocomposites with a Cloisite concentration of 3%. Inset shows the diffraction peak associated with the interlayer spacing for the pure organo-modified clay and the corresponding nanocomposite sample.

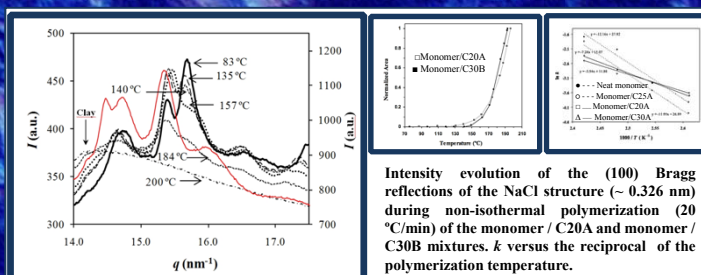


a) Changes in the infrared absorption bands at 3298, 1653, 1419 and 1166 cm⁻¹ of the poly(glc-alt-amh)/C20A nanocomposite during isothermal crystallization at 135°C.

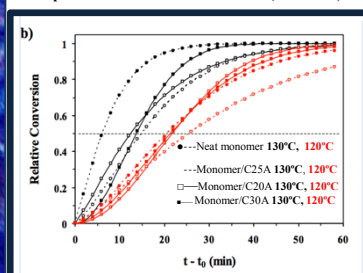
b) Time evolution of the relative crystallinity determined from absorbance measurements of the 3298 (■), 1653 (▲), 1419 (□) and 1166 (○) cm⁻¹ FTIR bands of the poly(glc-alt-amh)/C30B crystallization at 135°C.



WAXD profiles taken during the non-isothermal polymerization performed at a heating rate of 20 °C/min for two different mixtures. Insets show the evolution of the weak (100) NaCl reflection.



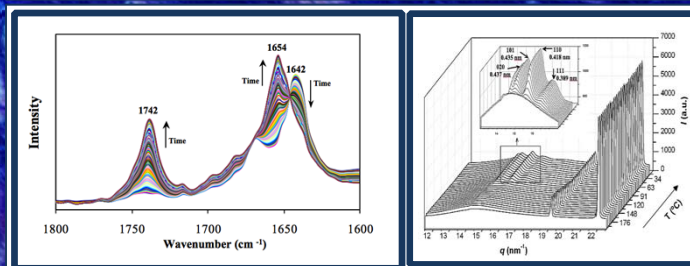
Intensity evolution of the (100) Bragg reflections of the NaCl structure (~0.326 nm) during non-isothermal polymerization (20 °C/min) of the monomer / C20A and monomer / C30B mixtures. *k* versus the reciprocal of the polymerization temperature. Representative WAXD profiles taken during a non-isothermal heating run (20 °C/min) performed with the monomer / C20A mixture and plotted in the *q* range where the main monomer reflections appeared (14 - 17.5 nm⁻¹). The selected temperatures correspond to the sample before (e.g. 83 °C) and after (e.g. 135 °C) occurrence of the monomer polymorphic transition, after being partially polymerized (e.g. 140, 157 and 184 °C) and at the end of the polycondensation reaction (e.g. 200 °C). In the last case only the amorphous halo and a small peak (see arrow) attributed to the clay could be observed. For the sake of completeness, the profile corresponding to a melt crystallized polymer sample taken at 140 °C is also shown (red curve).



Comparison of the conversion evolution between the neat monomer and its nanocomposites at the isothermal polymerization temperature of 130 °C and 120 °C. Data were calculated using Avrami equation: $a(t) = 1 - \exp(-Z(t-t_0)^n)$ and the corresponding crystallization kinetic parameters were deduced from FTIR absorbance measures of the 3298 cm⁻¹ band.

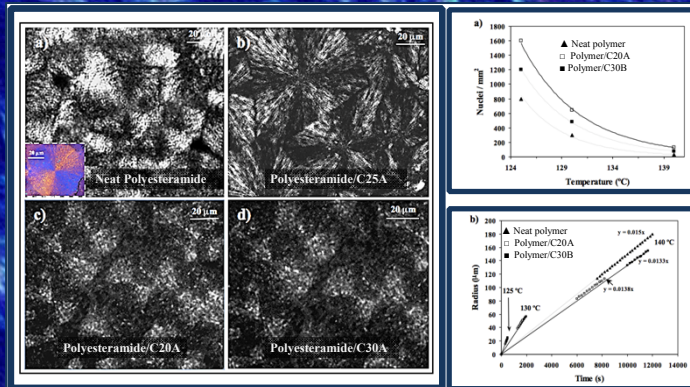
Table 1. Avrami Crystallization Kinetic Parameters.

Sample	$t_{1/2}$ (min)	Z (min ⁻¹)	n	k (min ⁻¹)
Neat polymer	0.048	$2.40 \cdot 10^5$	3.38	0.043
Nanocomposite with C20A	0.174	$3.40 \cdot 10^3$	3.01	0.153
Nanocomposite with C30B	0.149	$3.28 \cdot 10^3$	2.81	0.131



Absorbance FTIR spectra showing the evolution of the bands associated with the carboxylic ester group (1742 cm⁻¹) and amide I (1680-1620 cm⁻¹) during isothermal polymerizations of the monomer/C30B mixture at 110 °C.

WAXD profiles taken during the non-isothermal crystallization performed at a cooling rate of 20 °C/min and after non-isothermal polymerization of the monomer/C20A mixture at a heating rate of 20 °C/min. Insets show a magnification of the Bragg reflections corresponding to the poly(glc-alt-amh) structure.



Polarized optical micrographs showing the isothermal hot crystallizations of the neat poly(ester amide) and different nanocomposites at 130 °C. Inset shows a color micrograph of a speckled spherulite attained at 140 °C with the neat polymer sample. a) Variation in nucleation density with isothermal crystallization temperature for the neat polymer and its nanocomposites a). b) Plot of the radius of spherulites versus crystallization time for isothermal crystallizations at 125, 130 and 140 °C

Conclusions

Results indicate that C20A and C30B had a similar influence on the polymerization kinetics. Thus, the activation energy and the Arrhenius preexponential factor decreased compared to those calculated for the neat monomer. Clear differences were also found when using the C25A clay since, in this case, polymerization had similar activation energy to that determined for the neat monomer.

Crystallization: The incorporation of clay particles increased the overall rate kinetic constant due to the enhancement of the primary nucleation. On the contrary, the spherulitic growth rate was slightly disfavored by the clay.